Applied Catalysis B: Environmental 212 (2017) 50–58

Contents lists available at ScienceDirect

Applied Catalysis B: Environmental

journal homepage: www.elsevier.com/locate/apcatb

Mechanisms for the enhanced photo-Fenton activity of ferrihydrite modified with $BiVO_4$ at neutral pH

Tianyuan Xu[a,b], Runliang Zhu[a,*], Gangqiang Zhu[c], Jianxi Zhu[a], Xiaoliang Liang[a], Yanping Zhu[a,b], Hongping He[a]

[a] CAS Key Laboratory of Mineralogy and Metallogeny/Guangdong Provincial Key Laboratory of Mineral Physics and Material Research & Development, Guangzhou Institute of Geochemistry, Chinese Academy of Sciences, 511 Kehua Street, Guangzhou 510640, China
[b] University of Chinese Academy of Sciences, 19 Yuquan Road, Beijing 100049, China
[c] School of Physics and Information Technology, Shaanxi Normal University, Xi'an 710062, China

ARTICLE INFO

Article history:
Received 17 December 2016
Received in revised form 15 April 2017
Accepted 24 April 2017
Available online 25 April 2017

Keywords:
photo-Fenton
Semiconductor
Fe^{2+} generation
H_2O_2 decomposition

ABSTRACT

Heterogeneous photo-Fenton catalysts generally show very weak photo-Fenton activity at near-neutral pH because of the relatively low rate of Fe^{2+} regeneration. The aim of this work is to develop novel heterogeneous photo-Fenton catalysts, which can accelerate the regeneration of Fe^{2+} and thus have superior photo-Fenton activity at near-neutral pH. In this study, ferrihydrite (Fh) was modified with $BiVO_4$ to synthesize $BiVO_4$/Fh composites, and we expected that the photogenerated electrons from $BiVO_4$ would accelerate the regeneration of Fe^{2+} on Fh. Mechanistic investigation of H_2O_2 consumption showed that the introduction of $BiVO_4$ promoted the decomposition of H_2O_2 into reactive oxygen species (ROS). In addition, the presence of $BiVO_4$ deterred $O_2^{\bullet-}$ production and accelerated the formation of $^{\bullet}OH$, according to the results of ROS formation, as shown with EPR spectroscopy and fluorescent probes tools. Furthermore, the Fe^{2+} concentration on the surface of $BiVO_4$/Fh was higher than that on Fh based on the results of XPS characterization and quantitative measurement with a 1,10-phenanthroline spectrophotometric method. These results demonstrated that the introduction of $BiVO_4$ can accelerate the reduction of Fe^{3+} to Fe^{2+} by transferring photogenerated electrons from $BiVO_4$ to Fe^{3+} on the surface of Fh. Meanwhile, a higher decolorization efficiency of acid red 18 by $BiVO_4$/Fh than by Fh and pure $BiVO_4$ verified that the introduction of $BiVO_4$ can significantly enhance the photo-Fenton catalytic activity of Fh even at near-neutral pH. Overall, our work has important implications for understanding the photo-Fenton mechanisms on semiconductor modified heterogeneous photo-Fenton catalysts and confirms that the introduction of a semiconductor can enhance the photo-Fenton catalytic activity of heterogeneous photo-Fenton catalysts in acidic and neutral pH.

1. Introduction

A conventional Fenton reaction encompasses the reaction of hydrogen peroxide (H_2O_2) with Fe^{2+} under acidic conditions to form reactive oxygen species (ROS, usually $^{\bullet}OH$) that can degrade organic compounds (Eq. (1)) [1–4]; however, the main shortcoming of this reaction is that the recovery of Fe^{2+} through Eq. (2) is extremely slow [5]. Numerous studies have shown that light irradiation (< 580 nm) can be applied to accelerate the regeneration of Fe^{2+} (Eq. (4)) by the photolysis of Fe^{3+}, which is known as the photo-Fenton reaction [6,7]. However, the overall rate of the photoreduction of Fe^{3+} is still very low, especially under visible light irradiation (>420 nm) [3,8].

$$Fe^{2+} + H_2O_2 \rightarrow Fe^{3+} + {}^{\bullet}OH + OH^{-} \quad K \approx 70\,M^{-1}\,s^{-1} \tag{1}$$

$$Fe^{3+} + H_2O_2 \rightarrow Fe^{2+} + {}^{\bullet}OOH + H^{+} \quad K = 0.001\text{–}0.01\,M^{-1}\,s^{-1} \tag{2}$$

$$OOH \leftrightarrow O_2^{\bullet-} + H^{+} \quad (pKa = 4.8) \tag{3}$$

$$Fe(OH)^{2+} \xrightarrow{h\nu} Fe^{2+} + {}^{\bullet}OH \tag{4}$$

Another drawback of the photo-Fenton reaction is that its efficiency strongly depends on the solution pH, and the optimum pH is generally ~3, regardless of the target contaminants [9]. Under acidic conditions, the production of ROS in a heterogeneous photo-Fenton process mainly occurs in two ways. One is the reaction of the leached Fe from catalysts with H_2O_2 (i.e., a homogeneous photo-Fenton process); the other is the direct reaction between solid Fe

* Corresponding author.
E-mail address: zhurl@gig.ac.cn (R. Zhu).

http://dx.doi.org/10.1016/j.apcatb.2017.04.064
0926-3373/

on the catalysts and H_2O_2. However, at near-neutral pH, the production of ROS in a heterogeneous photo-Fenton process may only originate from the reaction between solid Fe on the catalysts and H_2O_2 because the leached Fe^{3+} in solution forms a ferric hydroxide sludge at pH ≥ 4 [2,10]. Additionally, the reduction of solid Fe^{3+} is much slower than that of aqueous Fe^{3+} [11]; hence, most of the photo-Fenton catalysts show very weak catalytic activity at high pH values [12]. For example, Feng et al. [13] found that the mineralization of Orange II by a bentonite-based Fe nanocomposite under UVC irradiation decreased significantly when the initial solution pH increased from 3.0 to 6.6. Therefore, one would expect that accelerating the reduction rate of Fe^{3+} on the surface of catalysts to Fe^{2+} may be a feasible way to enhance the catalytic activity of a heterogeneous photon-Fenton process at near-neutral pH.

Previous studies have shown that the reduction of Fe^{3+}, both in solution and on the surface of catalysts, can be accelerated by accepting electrons from excited dyes because some dyes readily undergo visible light-induced sensitization to donate electrons [14,15]. On the other hand, the photodecarboxylation of Fe-Carboxylic acid complexes via a ligand-to-metal charge transfer (LMCT) can also provide a quicker pathway for the reduction of Fe^{3+} to Fe^{2+} [16,17]. Meanwhile, several studies have shown that the in-situ addition of some organic chelating agents (e.g., tartaric acid, formic acid, and oxalate) into iron oxides (to form stable complexes) can also accelerate the reduction of Fe^{3+} to Fe^{2+} by modifying the redox potential of Fe^{3+}/Fe^{2+} [18–20]. However, both types of catalysts have relatively short life cycles, as the excited dye, Fe-Carboxylic acid complexes and organic chelating agents can be degraded in the photo-Fenton process.

Recently, several studies have showed that the introduction of semiconductor materials (e.g., TiO_2, $BiVO_4$) to the photo-Fenton system can enhance the degradation efficiency of the organic contaminants [21,22]. The generation of electrons in the conduction band (e_{CB}^-) and holes in the valence band (h_{VB}^+) of the semiconductor occur under light irradiation (Eq. (5)) [23]. The authors proposed that the semiconductor enhances the reduction of Fe^{3+} to Fe^{2+} by providing photogenerated electrons to Fe^{3+} (Eq. (6)) and then promotes H_2O_2 decomposition into •OH. However, other processes may also lead to the enhanced degradation efficiency of the organic contaminants. For example, H_2O_2 has also been proved to act as an electron acceptor for photogenerated electrons from the semiconductor, which can suppress the electron-hole recombination and increase ROS formation (Eq. (7)) [24,25]. In this case, more studies are urgently needed to clarify the role of the semiconductor in enhancing the degradation efficiency of the organic contaminants.

$$\text{Semiconductor} + h\nu \rightarrow e_{CB}^- + h_{VB}^+ \quad (5)$$

$$Fe^{3+} + e_{CB}^- \rightarrow Fe^{2+} \quad (6)$$

$$H_2O_2 + e_{CB}^- \rightarrow {}^{\bullet}OH + OH^- \quad (7)$$

In this work, $BiVO_4$/ferrihydrite composites with different $BiVO_4$ contents (0, 1, 3 and 5 wt%) were synthesized by growing ferrihydrite (Fh) on the surface of monoclinic $BiVO_4$. The influences of $BiVO_4$ on the photo-Fenton catalysis of Fh were examined by studying H_2O_2 decomposition, Fe^{2+} generation, and ROS formation at near-neutral pH. In addition, AR18 degradation was used to verify whether the presence of $BiVO_4$ improves the photo-Fenton catalytic activity of Fh. Overall, the results showed that the introduction of a semiconductor overcomes the major drawbacks of the photo-Fenton process, such as the low visible light utilization and strict pH range limits. Meanwhile, this work has important implications for understanding the photo-Fenton mechanisms on semiconductor-modified iron oxides and offers new insight into photo-Fenton catalysts synthesis.

2. Experimental sections

2.1. Materials

Acid red 18 (AR18, 85%) was purchased from the National Medicine Group Chemical Reagent Co., Ltd. (China) and used without further purification (Fig. S1). Hydrogen peroxide (H_2O_2, 30 wt%), ferric nitrate ($Fe(NO_3)_3{\cdot}9H_2O$), sodium hydroxide (NaOH), bismuth nitrate ($Bi(NO_3)_3{\cdot}5H_2O$), ammonium metavanadate (NH_4VO_3), sodium carbonate (Na_2CO_3), nitric acid (HNO_3), dimethyl sulfoxide (DMSO), potassium titanium oxalate ($K_2TiO(C_2O_4)_2{\cdot}2H_2O$), 1,10-phenanthroline monohydrate, acetic acid (CH_3COOH), and ammonium acetate (CH_3COONH_4) were of analytical grade and obtained from the Guangzhou Chemical Reagent Factory (Guangzhou, China). 4-Chloro-7-nitrobenz-2-oxa-1,3-diazole (NBD-Cl, 98%), potassium superoxide (KO_2, 96.5%), 5,5-dimethyl-1-pyrroline N-oxide (DMPO, 97%), terephthalic acid (TA, 99%), and 2-hydroxyterephthalic acid (TAOH, ≥98.0%) were purchased from Aladdin (China).

2.2. Preparation of catalyst

2.2.1. Synthesis of $BiVO_4$

Pure $BiVO_4$ was synthesized through a facile hydrothermal method, and the preparation process was as follows: $Bi(NO_3)_3$ (36 mmol) was dissolved in 150 mL of a 2.0 M HNO_3 solution, and then, 150 mL of NH_4VO_3 (36 mmol) was added dropwise into the $Bi(NO_3)_3$ solution under stirring to form a final suspension. The suspension pH value was then adjusted to 2.0 with 2.0 M $NH_3{\cdot}H_2O$. After being stirred for approximately 2 h, the suspension was transferred into a 500-mL Teflon-lined autoclave and heated to 200 °C for 24 h. After cooling the autoclave to room temperature, the products were collected, centrifuged, and washed.

2.2.2. Synthesis of $BiVO_4$/Fh

$BiVO_4$ was first ultrasonically treated for 30 min, and the synthesis of $BiVO_4$/Fh was as follows: $Fe(NO_3)_3$ (1 M, 40 mL) and NaOH (6 M, 20 mL) were slowly and simultaneously titrated into a 50-mL suspension containing a certain amount of $BiVO_4$ (0.043, 0.128, or 0.214 g) under vigorous stirring, and the pH value was controlled at 7 ± 0.1. After continuous stirring for another 3 h, the products were centrifuged and washed. According to the $BiVO_4$ content, the resulting materials were labeled as 1%$BiVO_4$/Fh, 3%$BiVO_4$/Fh, and 5%$BiVO_4$/Fh.

For comparison, pure Fh was synthesized using similar processes without addition of $BiVO_4$. All of the obtained samples were freeze-dried under −40 °C and pulverized to pass through a 100-mesh sieve.

2.3. Characterization

Powder X-ray diffraction (XRD) measurements were performed on an X-ray diffractometer (Bruker D8 ADVANCE) with Cu Kα irradiation (40 kV, 40 mA). All of the XRD patterns were obtained from 10° and 80° with a scan speed of 2°/min. X-ray photoelectron spectroscopy (XPS) data were obtained by a Thermo Fisher Scientific K-Alpha spectrometer. The C1s peak from the adventitious carbon-based contaminant with a binding energy of 284.8 eV was used as the reference for calibration. Morphological observations were performed by a scanning electron microscope (SEM, SU8010, Hitachi), and the surface chemical composition of the samples was semi-quantitatively evaluated through SEM linked with Oxford Inca250 energy dispersive X-ray spectroscopy (EDS) analysis.

Steady-state UV–visible diffuse reflectance spectra (DRS) were measured using a UV–visible spectrophotometer (Shimadzu UV-2550 double-beam digital spectrophotometer). PEC charac-

terization was performed with a CHI electrochemical analyzer (CHI6001) using the standard three-electrode mode with a 0.05 M Na_2SO_4 solution as the electrolyte. The $BiVO_4$ photoanode was used as the working electrode; a Pt sheet served as the counter-electrode. A Ag/AgCl (saturated KCl) electrode was used as the reference electrode at room temperature. Nitrogen adsorption-desorption isotherms were determined on a Micromeritics ASAP 2020 M instrument. All of the samples were degassed for 12 h at 60 °C prior to N_2 adsorption measurements. The specific surface areas (SSA) of the samples were calculated using the multiple-point Brunauer-Emmett-Teller (BET) method.

2.4. Photocatalytic tests and analytical methods

The photocatalytic performance of the synthesized photocatalysts was investigated in a multi-tube agitated reactor (PCX50A Discover, Beijing Perfectlight Technology Co., Ltd, Beijing, China). A 5 W LED lamp (450 nm, 0.7 mW/cm^2) was used as a cold light source. Photocatalyst at a concentration of 4×10^{-1} g/L (except for pure $BiVO_4$, 6×10^{-2} g/L, thrice as the amount of $BiVO_4$ on 5%$BiVO_4$/Fh) was added into 50 mL of ultrapure water or an AR solution (5×10^{-5} M) with magnetic stirring. The initial pH value of the solution was adjusted using 0.1 M NaOH or HNO_3. Subsequently, H_2O_2 (1×10^{-2} M) was added and visible light was used to immediately irradiate the suspension. The recycling experiment of 3%$BiVO_4$/Fh was started in the same way. After each reaction cycle, the suspension was centrifuged, supernatant was analyzed, and solid was collected for the next run.

At given time intervals, 1-mL aliquots were sampled and filtered immediately with 0.45-μm membrane filters. The absorbance of AR18 was measured at 509 nm via a UV–vis spectrophotometer (759S, Shanghai JingHua Instrument Co. Ltd., China). Total organic carbon (TOC) was measured by a TOC analyzer (Shimadzu TOC-V CPH, Japan) equipped with an autosampler. The concentration of H_2O_2 was determined by adding 3 mL of $K_2TiO(C_2O_4)_2$ (10 mM in 2.4 M H_2SO_4), which forms an orange complex (pertitanic acid) with a maximum absorption at 400 nm [26]. The amount of total Fe ions leached from catalysts into the solution was determined by atomic absorption spectrophotometry (AAS, PerkinElmer AAnalyst 400, America). For Fe(II) analysis, after different reaction times, the catalysts (0.02 g) were collected by filtration and added to 25-mL colorimetric tubes. Then, 0.2 g of Na_2CO_3, 2 mL of HCl (1:1), 1 mL of 1 M NH_4F, 5 mL of 1,10-phenanthroline (3×10^{-2} M), and 10 mL of a CH_3COONH_4–CH_3COOH buffer solution (pH 4.2) were added to the centrifuge tubes [27,28]. After dilution to 25 mL and 15 min of color development, the absorbance of the samples at 510 nm was analyzed on a UV–vis spectrophotometer.

2.5. Analysis of reactive oxygen species

Electron paramagnetic resonance (EPR) was used to qualitatively analyze the formation of •OH and $O_2^{\bullet-}$. EPR signals of radicals trapped by DMPO (20 mM) were recorded at ambient temperature on a Bruker E500 spectrometer. The settings for the EPR spectrometer were as follows: center field, 3480 G; sweep width, 50 G; microwave frequency, 9.84 GHz; modulation frequency, 100 kHz; and power, 6.33 mW.

The concentrations of •OH and $O_2^{\bullet-}$ were quantified by a fluorescence method using TA (4 mM) and NBD-Cl (100 uM) as probes. After filtration, 3 mL of the reaction product of •OH and TA was measured with a Hitachi F-4500 fluorescence spectrometer at 425 nm (excited at 312 nm) [29]; while 1 mL of the reaction product of $O_2^{\bullet-}$ and NBD-Cl was immediately added to 2 mL of acetonitrile, and their intermixture was immediately measured at 550 nm (excited at 470 nm) [30].

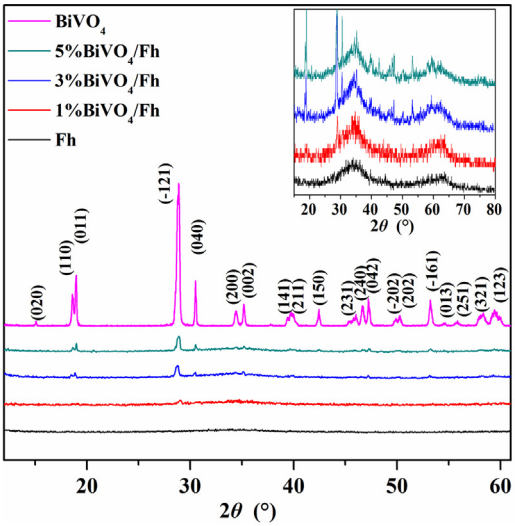

Fig. 1. The XRD patterns of samples.

3. Results and discussion

3.1. Structural characterization results

The XRD patterns of the pure $BiVO_4$ (Fig. 1) revealed that $BiVO_4$ is consistent with the structure of monoclinic scheelite (JCPDS No. 14-0688). In addition, the XRD patterns of $BiVO_4$/Fh showed characteristic reflections at 18.9°, 28.8°, and 30.5°(2θ) except for 1%$BiVO_4$/Fh (only the characteristic reflection at 28.8°), suggesting that $BiVO_4$ existed in the composites. On the other hand, all of the samples showed two broad peaks at 35° and 63° (insert of Fig. 1), consistent with previous reports for pure 2-line Fh [31], implying that the presence of $BiVO_4$ did not significantly affect the structure of Fh. Additionally, the BET data (Table 1) showed that the SSA of the $BiVO_4$/Fh composites was slightly smaller than that of Fh. Meanwhile, the SSA of $BiVO_4$/Fh decreased slightly with the increasing content of $BiVO_4$, probably because the SSA of pure $BiVO_4$ was too small (only 5.2 m^3/g).

Pure $BiVO_4$ microcrystals showed a truncated tetragonal bipyramid morphology (Fig. 2), while pure Fh showed aggregations of small particles. Additionally, it can be observed that $BiVO_4$ was present in 5%$BiVO_4$/Fh, but the 1%$BiVO_4$/Fh and 3%$BiVO_4$/Fh composites were morphologically similar to Fh. According to a previous study, Fh should be an approximately spherical particle with a diameter of less than 3 nm, but the nanoparticles easily aggregated into micrometer-sized particles [32]. On the other hand, $BiVO_4$/Fh composites were synthesized by growing Fh on the surface of $BiVO_4$, so the Fh on the surface of $BiVO_4$ hindered the observation of $BiVO_4$ in $BiVO_4$/Fh images with a low $BiVO_4$ content.

The EDS patterns of samples (Fig. S2 and Table 1) showed that the atomic ratio of Bi/V was close to 1, which is in agreement with the theoretical ratio of $BiVO_4$. The Bi and V contents were 0.22 (at%) on 5%$BiVO_4$/Fh and 0.14 (at%) on 3%$BiVO_4$/Fh. However, the Bi and V contents on 1%$BiVO_4$/Fh could not be determined because the content of $BiVO_4$ was too low to be detected by EDS. Meanwhile, EDS mapping was selected for further analysis of the elemental distribution of 3%$BiVO_4$/Fh. As shown in Fig. 2, Bi, V, Fe, and O were well distributed in the respective regions.

The UV–vis DRS of the samples (Fig. 3) showed that pure $BiVO_4$ absorbs solar energy below 540 nm, and pure Fh exhibited absorption even up to 650 nm. However, the absorption bands of $BiVO_4$/Fh showed a slight blue shift compared to that of pure $BiVO_4$ and a stronger UV–vis light photoabsorption than that of pure Fh. Moreover, the UV–vis light photoabsorption of the composites increased

Table 1
The structural characteristics of various samples.

Samples	Fe Atomic (at%)	O Atomic (at%)	Bi Atomic (at%)	V Atomic (at%)	SSA (m^3/g)
Fh	21.66	78.34	–	–	301.9
1%$BiVO_4$/Fh	14.62	85.34	–	–	293.2
3%$BiVO_4$/Fh	13.00	86.72	0.14	0.14	288.1
5%$BiVO_4$/Fh	12.13	87.43	0.22	0.22	282.8

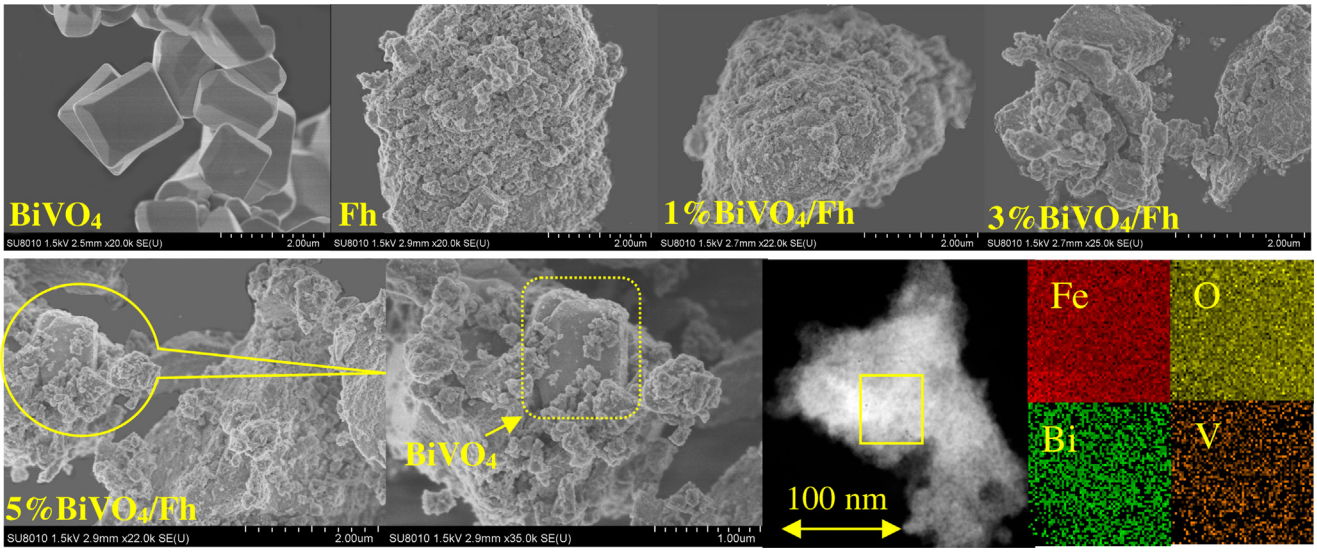

Fig. 2. SEM images of samples and TEM-EDS mapping images of 3%$BiVO_4$/Fh.

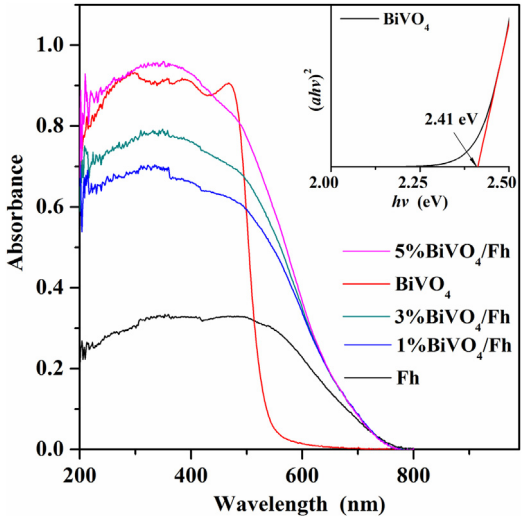

Fig. 3. UV–vis diffuse reflectance spectra and (inset) plots of $(ahv)^2$ versus the photon energy (hv) of samples.

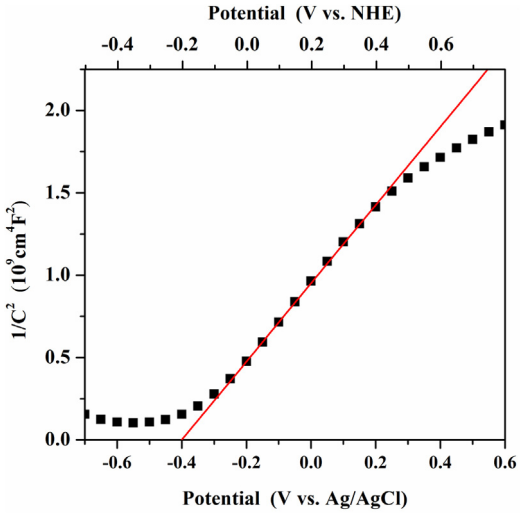

Fig. 4. Mott–Schottky plots of $BiVO_4$ collected at a frequency of 1 kHz.

with increasing $BiVO_4$ content. In addition, the band gap transition of $BiVO_4$ was determined from the plots of $(ahv)^2$ against (hv) (inset of Fig. 3), corresponding to a band gap energy of 2.41 eV, which was in accordance with previous reports [33,34].

The Mott-Schottky test was conducted to calculate the flatband potential (E_{fb}) of pure $BiVO_4$. Fig. 4 shows that pure $BiVO_4$ presented a positive slope in Mott–Schottky plots, as expected for an n-type semiconductor [35]. E_{fb}, obtained by extrapolating the curve to $1/C^2 = 0$, was estimated to be −0.20 V vs. NHE. Generally, for n-type semiconductors, the conduction band potential is nearly equal to the flat-band potential [36]. Thus, the conduction band potential of pure $BiVO_4$ was −0.2 V vs. NHE, which was lower than the redox potential of Fe^{3+}/Fe^{2+} ($E^0(Fe^{3+}/Fe^{2+}) = 0.77$ V vs. NHE) [37]. Hence, in theory, $BiVO_4$ can accelerate the reduction of Fe^{3+} to Fe^{2+} by transferring photogenerated electrons from $BiVO_4$ to Fe^{3+} on the surface of Fh.

3.2. H_2O_2 consumption

It is well known that the study of H_2O_2 consumption is crucial for evaluating the photo-Fenton catalytic efficiency. Fig. 5 depicts the consumption of H_2O_2 by samples as a function of reaction time under various conditions. With only visible light irradiation, H_2O_2 did not exhibit significant consumption, i.e., nearly 5.6% H_2O_2

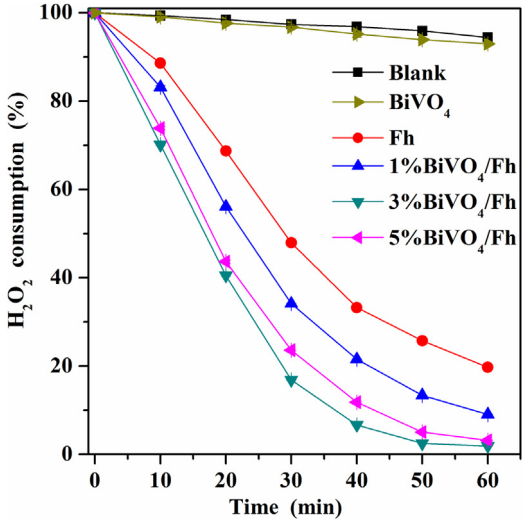

Fig. 5. H_2O_2 consumption over samples at an initial ultrapure water pH of 6.5.

decomposition after 60 min of reaction. However, the addition of photo-Fenton catalysts could significantly accelerate the consumption of H_2O_2. In the presence of Fh, the consumption of H_2O_2 reached 80.2% after 60 min of reaction. The introduction of $BiVO_4$ further enhanced the consumption of H_2O_2, 90.9% for 1%$BiVO_4$/Fh and 98.1% for 3%$BiVO_4$/Fh. However, the consumption of H_2O_2 showed a slight decrease when the $BiVO_4$ content was further increased, i.e., 96.2% for 5%$BiVO_4$/Fh, which may be due to the easy aggregation of $BiVO_4$/Fh at high relative contents (Fig. S3).

Ge et al. have reported that the degradation rate of RhB was greatly enhanced when H_2O_2 was introduced into the $BiVO_4$/sunlight system because H_2O_2 is an efficient electron scavenger. They also found that the presence of Fe^{3+} prevented the electron-hole recombination by accepting photogenerated electrons from $BiVO_4$ [25]. Hence, the possible reasons for enhanced H_2O_2 consumption by $BiVO_4$/Fh may be attributed to direct consumption by photogenerated electrons from $BiVO_4$. On the other hand, accelerated Fe^{3+} reduction to Fe^{2+} by accepting photogenerated electrons from $BiVO_4$ can enhance the consumption of H_2O_2 as well. However, in this study, H_2O_2 consumption was slightly increased by pure $BiVO_4$ compared with the photolysis of H_2O_2, implying that direct consumption of H_2O_2 by $BiVO_4$ was not the dominant reason for enhanced H_2O_2 consumption. However, if it was the other reason, the concentration of Fe^{2+} on $BiVO_4$/Fh should be increased after visible light irradiation, which will be discussed below.

3.3. Fe^{2+} regeneration

Because the production of Fe^{2+} is crucial to verifying the reasons for enhanced H_2O_2 consumption, the concentration of Fe^{2+} was determined on samples and the supernatant during the reaction. The concentrations of Fe^{2+} and total Fe in the supernatant were found to be lower than the limit of detection (0.06 mg/L and 0.1 mg/L, respectively), implying that both of Fh and $BiVO_4$/Fh were stable at near-neutral pH.

Fig. 6 shows the Fe^{2+} concentration on the catalysts at an initial solution pH of 6.5. The reduction of Fe^{3+} to Fe^{2+} was observed on all samples after the addition of H_2O_2 (Fig. 6A). The concentration of Fe^{2+} increased dramatically over 20 min and then decreased, and this behavior was in accordance with that observed by Ma [11].

Interestingly, the concentration of Fe^{2+} on all samples increased with time under visible light irradiation when H_2O_2 was absent (Fig. 6B) in addition to Fe^{2+} generation with H_2O_2 addition. This suggests that the generated Fe^{2+} quickly reacted with H_2O_2, but once H_2O_2 was absent, the generated Fe^{2+} was relatively long-lived and accumulated on the catalysts. In addition, the concentration of Fe^{2+} on $BiVO_4$/Fh was much higher than that on Fh, independent of H_2O_2 addition. Furthermore, the concentration of Fe^{2+} on $BiVO_4$/Fh increased with the $BiVO_4$ content, but decreased when the $BiVO_4$ content was further increased to 5%, which was the same trend as H_2O_2 consumption.

According to previous studies, Fe^{3+} can act as an acceptor of photogenerated electrons from a semiconductor (such as $BiVO_4$, TiO_2 and Ag_3PO_4) during the photocatalytic process to suppress electron-hole recombination [25,38,39]. Therefore, in this work, the high Fe^{2+} concentration on $BiVO_4$/Fh was attributed to the presence of $BiVO_4$, which can accelerate the reduction of Fe^{3+} to Fe^{2+} by contributing photogenerated electrons to Fe^{3+} under visible light irradiation. This result also verified that the enhanced H_2O_2 consumption described above was mainly due to accelerated Fe^{3+} reduction to Fe^{2+} through acceptance of photogenerated electrons from $BiVO_4$.

To further demonstrate the advantage of $BiVO_4$ over $BiVO_4$/Fh composites, Fe^{2+} formation on fresh and used samples was further characterized by XPS. As shown in Fig. S4, the Fe $2p_{3/2}$ XPS spectra of fresh Fh showed two peaks with binding energies of 710.4 and 711.5 eV, both of which can be assigned to Fe^{3+} [40]. However, no significant Fe^{2+} signal appeared after visible light irradiation, regardless of the H_2O_2 content, perhaps because the Fe^{2+} concentration was too low to be detected by XPS. As for 3%$BiVO_4$/Fh, no significant Fe^{2+} signal appeared after the addition of H_2O_2, as with Fh, but a small Fe^{2+} signal with a binding energy of 709.6 eV [40] was observed after visible light irradiation for 60 min. Overall, this result further illustrates that reduction of Fe^{3+} on the surface of $BiVO_4$/Fh to Fe^{2+} was achieved by accepting photogenerated electrons from $BiVO_4$.

3.4. ROS identification

Given that the generation of ROS is crucial to the photo-Fenton catalytic efficiency, EPR spectroscopy analysis was applied to detect the formation of $^{\bullet}OH$ and $O_2^{\bullet-}$. As shown in Fig. S5, a quartet of signals from the DMPO–$^{\bullet}OH$ adducts ($a_N = a_{H\beta} = 14.96$ G) with relative intensities of 1:2:2:1 were detected in the water phase [41]. In the presence of methanol, a four-line ESR signal with an intensity ratio of nearly 1:1:1:1 was clearly observed, which was characteristic of the DMPO-$O_2^{\bullet-}$ adduct [42]. The EPR results suggested that both $^{\bullet}OH$ and $O_2^{\bullet-}$ were generated in the heterogeneous photo-Fenton process.

To provide further evidence of $^{\bullet}OH$ and $O_2^{\bullet-}$ production, TA and NBD-Cl were used as probes for the quantitative assay of the $^{\bullet}OH$ and $O_2^{\bullet-}$ concentrations in the heterogeneous photo-Fenton process, respectively. As shown in Fig. 7, a reaction suspension with TA, H_2O_2 and Fh exhibited $^{\bullet}OH$ production, as evidenced by an increase in fluorescence emission with increasing time, and the $^{\bullet}OH$ concentration reached 15.4 umol/L after 60 min of reaction. When $BiVO_4$/Fh was the photo-Fenton catalyst, the $^{\bullet}OH$ production and fluorescence emission (by 3%$BiVO_4$/Fh) were obviously improved compared with those by Fh, suggesting that $BiVO_4$ can encourage the formation of $^{\bullet}OH$. Furthermore, $^{\bullet}OH$ production first increased with the increasing content of $BiVO_4$ (the highest $^{\bullet}OH$ concentration can reach 28.3 umol/L by 3%$BiVO_4$/Fh), but began to decrease when the content of $BiVO_4$ was further increased to 5%.

However, the production of $O_2^{\bullet-}$ (Fig. 8) was lower than the production of $^{\bullet}OH$ by as much as three-fold. This result indicated that $^{\bullet}OH$ was the dominant ROS in the heterogeneous photo-Fenton process, which agrees well with most previous results [21,32,43]. A suspension composed of NBD-Cl, H_2O_2 and Fh exhib-

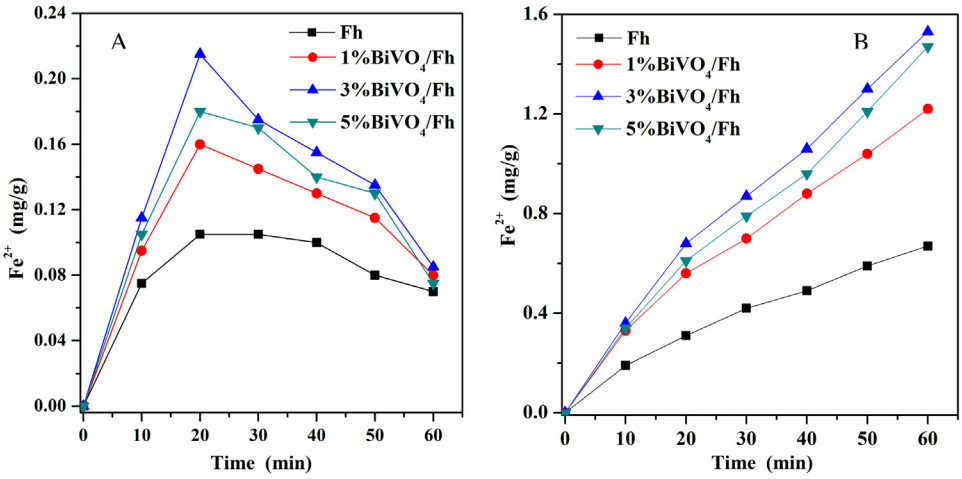

Fig. 6. Concentration of Fe^{2+} on the samples at an initial ultrapure water pH of 6.5 with (A) or without (B) added H_2O_2.

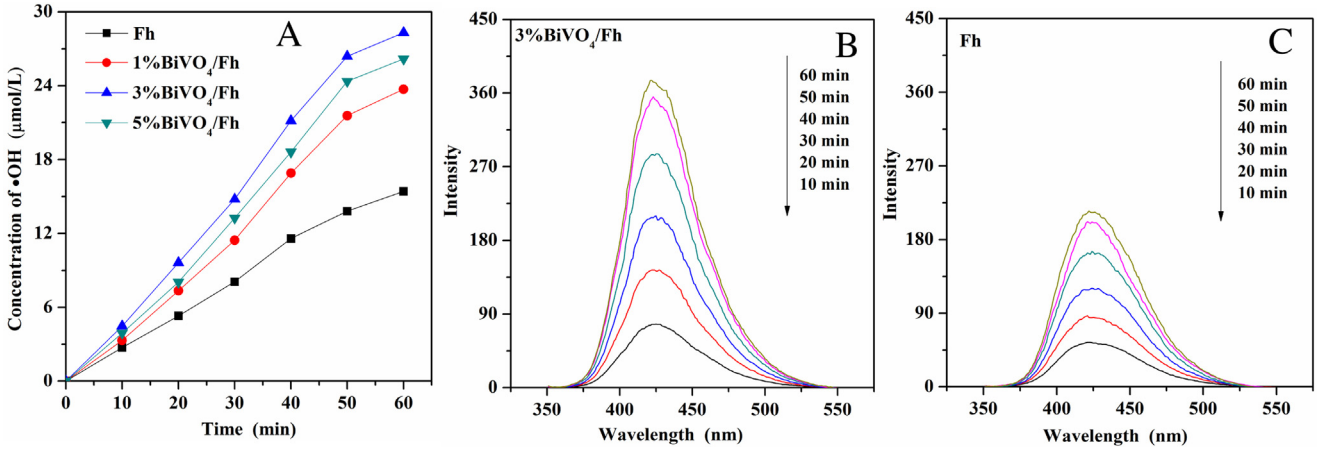

Fig. 7. The concentration of •OH in the heterogeneous photo-Fenton (A) and fluorescence emission spectra of TA–•OH adducts (B, C) at an initial ultrapure water pH of 6.5.

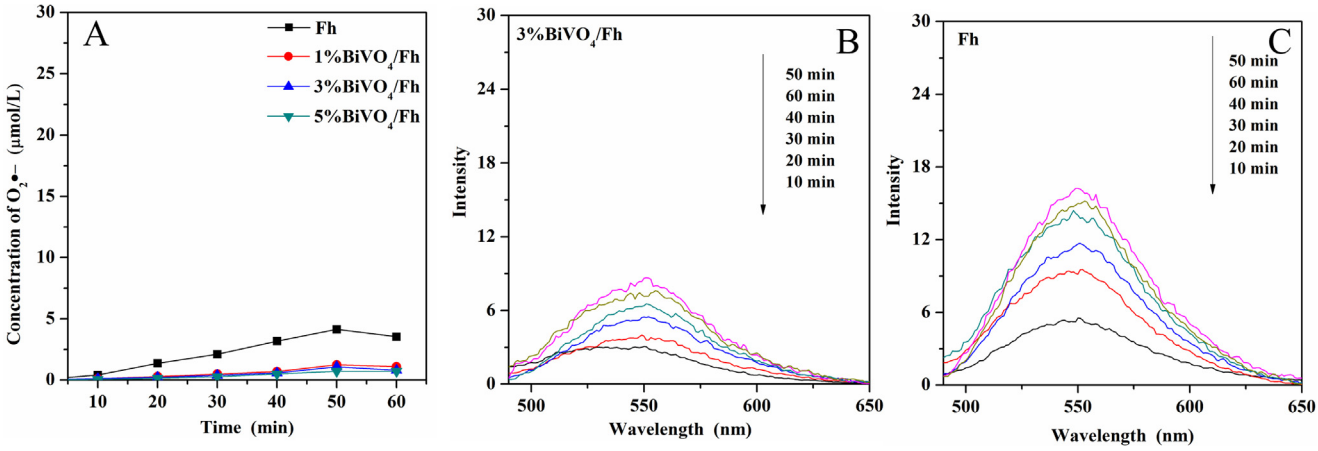

Fig. 8. The concentration of $O_2^{\bullet-}$ in the heterogeneous photo-Fenton (A) and fluorescence emission spectra of NBD-Cl–$O_2^{\bullet-}$ adduct (B, C) at an initial ultrapure water pH of 6.5.

ited an increase in fluorescence emission with time, and the highest $O_2^{\bullet-}$ concentration reached 4.1 umol/L. Nevertheless, a decrease in $O_2^{\bullet-}$ production was observed when introducing $BiVO_4$ to Fh, and $BiVO_4$/Fh exhibited a lower fluorescence emission than that of Fh, suggesting that $BiVO_4$ may deter $O_2^{\bullet-}$ production.

It is well known that the reaction between H_2O_2 and Fe^{2+} is the major approach for producing •OH in the photo-Fenton process (Eq. (1)). However, H_2O_2 can react with Fe^{3+} to form $O_2^{\bullet-}$ in aqueous solution when the pH value is higher than 4.8 (Eqs. (2), (3)). For pure $BiVO_4$, due to its low conduction band position (−0.2 V vs.

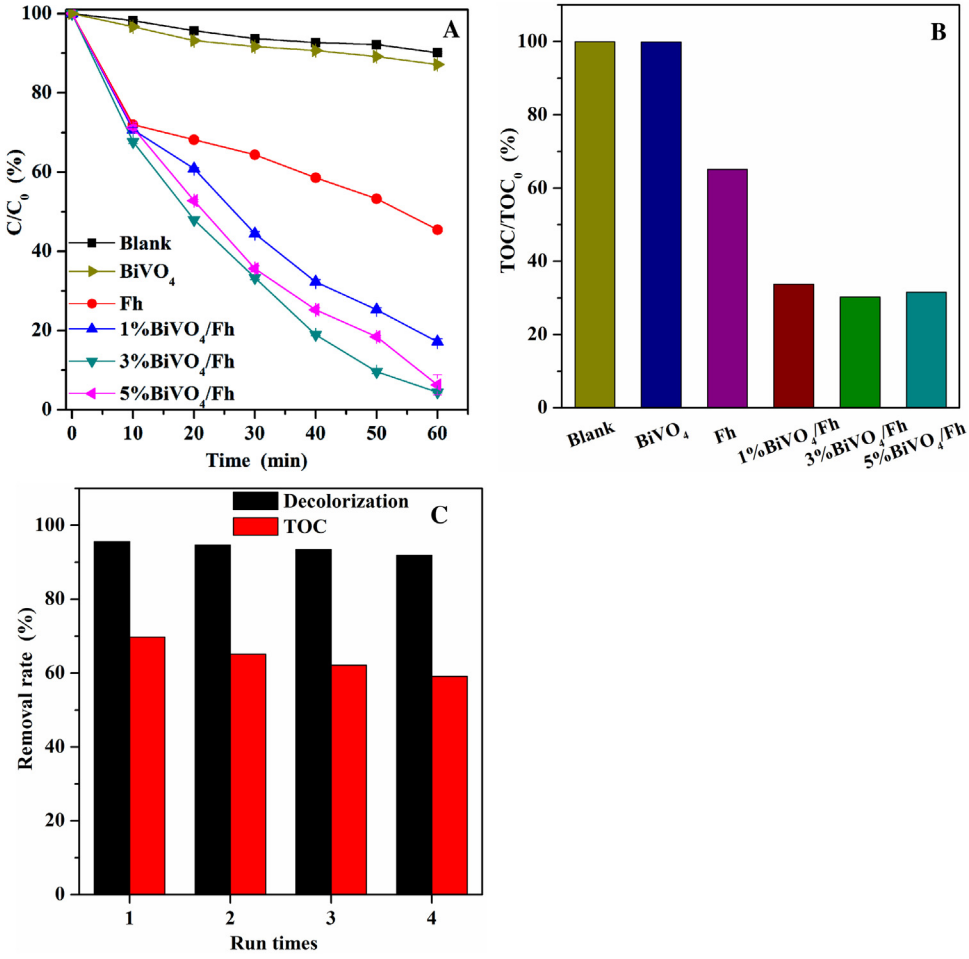

Fig. 9. Decolorization (A) and mineralization (B) of AR18 under visible light irradiation with added H_2O_2, and (C) the stability of 3%$BiVO_4$/Fh in the photo-Fenton process at an initial AR18 solution pH of 6.5.

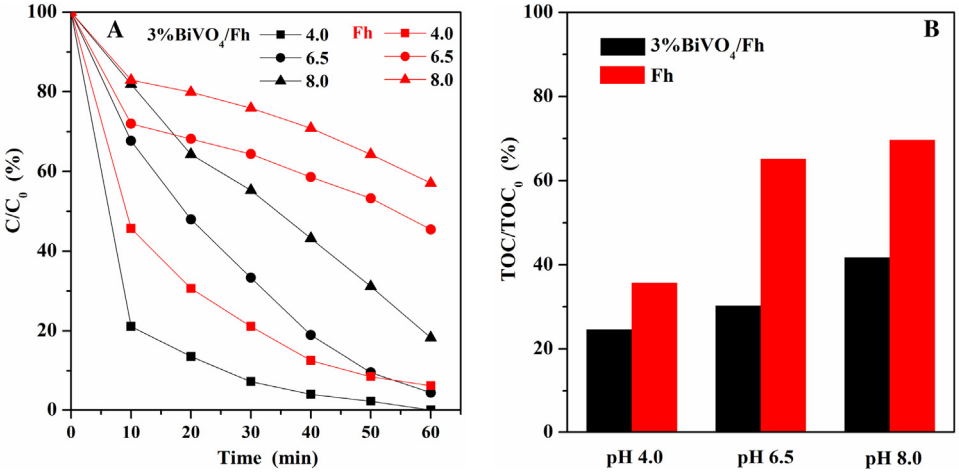

Fig. 10. Effect of pH on decolorization (A) and mineralization (B) of AR18 over Fh and 3%$BiVO_4$/Fh during photo-Fenton process.

NHE), e_{CB}^- may facilitate the multiple-electron reduction reaction of O_2 to form $O_2^{\bullet-}$ (Eq. (8), $E^0(O_2/O_2^{\bullet-}) = -0.046$ V vs. NHE) [44,45]. However, once $BiVO_4$ is co-located with other electron accepters, such as Fe^{3+}, e_{CB}^- would preferentially transfer to other electron accepters rather than the dissolved O_2.

In the case of $BiVO_4$/Fh, $BiVO_4$ contributed e_{CB}^- to Fe^{3+} on the surface of Fh, which markedly inhibited the processes of Eqs. (2), (3), (8), but accelerated the process of Eq. (1), and ultimately reduced the $O_2^{\bullet-}$ concentration, but encouraged the formation of •OH after the introduction of $BiVO_4$. The results of ROS identification better illustrate that the presence of $BiVO_4$ can accelerate the reduction of Fe^{3+} to Fe^{2+} on $BiVO_4$/Fh.

$$O_2 + e_{CB}^- \rightarrow O_2^{\bullet-} \quad (8)$$

3.5. AR18 degradation

To validate the photo-Fenton catalytic activity of samples under near-neutral pH, several photocatalytic experiments were performed for AR18 degradation under various conditions. Under dark conditions (Fig. S6), it appeared that approximately 20% AR18 (much the same with TOC removal rate) could adsorb to the surface of Fh in 60 min. On the other hand, adsorption of AR18 decreased slightly with the introduction of $BiVO_4$ compared to Fh, which was in accordance with the SSA of samples.

Under visible light irradiation (Fig. 9), approximately 10% AR18 (negligible TOC removal rate) was removed by adding H_2O_2 due to H_2O_2 photolysis, which produced •OH. For pure $BiVO_4$, e_{CB}^- may facilitate the multiple-electron reduction reaction of O_2 to form $O_2^{\bullet-}$, water oxidation by h_{VB}^+ could release •OH, and the h_{VB}^+ can also be used as reactive species in direct charge transfer oxidation of organics. But the addition of $BiVO_4$ did not obviously improve the degradation of AR18 in our study, which indicated that pure $BiVO_4$ had a weak ability for catalytic decolorization and mineralization of AR18 under the tested conditions.

However, once photo-Fenton catalysts were introduced, degradation of AR18 obviously increased, and faster AR18 degradation contributed to faster •OH production from the reaction between H_2O_2 and photo-Fenton catalysts. As for pure Fh, approximately 55% decolorization and 35.8% TOC removal rates of AR18 were reached. However, the degradation rate of AR18 reached 82.8% (66.3% for TOC removal rate) with 1%$BiVO_4$, and this increased to 95.6% (69.7% for TOC removal rate) when the $BiVO_4$ content increased to 3%, but underwent a slight decrease when the $BiVO_4$ content further increased to 5% (93.7% decolorization and 68.5% TOC removal rate of AR18). The trend of AR18 degradation by $BiVO_4$/Fh with different $BiVO_4$ contents was the same as the trend of H_2O_2 consumption and Fe^{2+} regeneration. The results of AR18 degradation verified that the presence of $BiVO_4$ could significantly enhance the photo-Fenton catalytic activity of Fh, even at near-neutral pH. In addition, the Fe concentrations (in the solution) in each AR18 degradation system at an initial solution pH of 6.5 were lower than the limit of AAS detection (Table S1). Hence, sludge should not be formed in these catalytic systems.

As is well known, the stability of a catalyst is a key issue for its practical application. The results of the stability test of 3%$BiVO_4$/Fh showed that the decolorization (90.1%) and TOC removal rate of AR18 (59.1%) were not obviously decreased after being used for 4 cycles (Fig. 9C), and the Fe concentration in the solution was still lower than the limit of AAS detection (Table S1), implying that 3%$BiVO_4$/Fh was stable.

In addition, the effect of pH on degradation of AR18 over Fh and 3%$BiVO_4$/Fh during the photo-Fenton process was investigated (Figs. 10, S7). The results showed that AR18 was decolorized and mineralized most efficiently at an initial pH of 4.0 under visible light irradiation, both for Fh and 3%$BiVO_4$/Fh. However, the decolorization and TOC removal rates of AR18 were decreased with the pH increasing from 4.0 to 8.0, which may have two causes.

One cause is due to the reduction of solid Fe^{3+}, which is much slower than that of aqueous Fe^{3+} [11]. At an initial solution pH of 4.0, obvious Fe leaching from Fh and 3%$BiVO_4$/Fh was observed, but no significant Fe in solution was detected at an initial pH of 6.5 or 8.0, which meant that the reduction of Fe^{3+} was faster at pH 4.0 than at pH 6.5 or 8.0. On the other hand, the oxidation potential of •OH decreases with increasing pH. It ranges from 2.65 to 2.80 V at pH 3 and reaches 1.90 V at pH 7, where the free energy of neutralization is not available [46], which means that •OH is a weaker oxidant at neutral pH than at near-acidic pH. Therefore, AR18 was decolorized and mineralized most efficiently at an initial pH of 4.0.

Nevertheless, in either acidic or neutral solutions, degradation of AR18 by 3%$BiVO_4$/Fh was more effective than that by Fh, even though Fe leaching from 3%$BiVO_4$/Fh (0.105 mg/L) was lower than that from Fh (0.181 mg/L) at an initial solution pH of 4.0. Hence, the introduction of a semiconductor can enhance the photo-Fenton catalytic activity of heterogeneous photo-Fenton catalysts both at acidic and neutral pHs.

4. Conclusion

In this study, the effects of $BiVO_4$-modified Fh on the photocatalytic mechanism were explored. Mechanistic investigations of H_2O_2 decomposition and Fe^{2+} generation verified that the induction of $BiVO_4$ to Fh can enhance H_2O_2 consumption and Fe^{2+} regeneration. Meanwhile, the results further proved that enhanced H_2O_2 consumption is due to accelerated Fe^{3+} reduction by accepting photogenerated electrons from $BiVO_4$, rather than by direct consumption of H_2O_2 by $BiVO_4$. Analyzing the formation of ROS results showed that the presence of $BiVO_4$ suppressed the reaction of Fe^{3+} and H_2O_2, which decreased the concentration of $O_2^{\bullet-}$, but increased the formation of •OH. Additionally, the higher decolorization efficiency of AR18 by $BiVO_4$/Fh at near-neutral pH, compared to that by Fh and pure $BiVO_4$, verified that the introduction of $BiVO_4$ significantly enhanced the photo-Fenton catalytic activity of Fh even at near-neutral pH. Overall, our work demonstrated that the enhanced photo-Fenton activity was due to the presence of $BiVO_4$, which can accelerate the reduction of Fe^{3+} to Fe^{2+} by transferring photogenerated electrons from $BiVO_4$ to Fe^{3+} on the surface of Fh. In addition, this work is a useful reference for enhancing the photo-Fenton catalytic activity in the design and fabrication of environment-friendly photo-Fenton catalysts.

Acknowledgements

This work was financially supported by National Natural Science Foundation of China (41572031), National Youth Top-notch Talent Support Program, Newton Advanced Fellowship (NA150190), CAS/SAFEA International Partnership Program for Creative Research Teams (20140491534), and Guangdong Provincial Youth Top-notch Talent Support Program (2014TQ01Z249).

Appendix A. Supplementary data

Supplementary data associated with this article can be found, in the online version, at http://dx.doi.org/10.1016/j.apcatb.2017.04.064.

References

[1] E. Neyens, J. Baeyens, J. Hazard. Mater. 98 (2003) 33–50.
[2] N.S. Ai, B.H. Hameed, Desalination 269 (2011) 1–16.
[3] J. Herney-Ramirez, M.A. Vicente, L.M. Madeira, Appl. Catal. B: Environ. 98 (2010) 10–26.
[4] H.J.H. Fenton, J. Chem. Soc. Trans. 65 (1894) 899–910.
[5] C. Lee, D.L. Sedlak, J. Mol. Catal. A: Chem. 311 (2009) 1–6.
[6] N. Klamerth, S. Malato, A. Agüera, A. Fernández-Alba, Water Res. 47 (2012) 833–840.
[7] A.D. Bokare, W. Choi, J. Hazard. Mater. 275 (2014) 121–135.
[8] Y. Ju, Y. Yu, X. Wang, M. Xiang, L. Li, D. Deng, D.D. Dionysiou, J. Hazard. Mater. 323 (2017) 611–620.
[9] C. Cai, Z. Zhang, J. Liu, N. Shan, H. Zhang, D.D. Dionysiou, Appl. Catal. B: Environ. 182 (2016) 456–468.
[10] X. Tang, Y. Liu, Dyes Pigm. 134 (2016) 397–408.
[11] Z. Ma, L. Ren, S. Xing, Y. Wu, Y. Gao, J. Phys. Chem. C 119 (2015) 23068–23074.
[12] R. Gonzalez-Olmos, M.J. Martin, A. Georgi, F.D. Kopinke, I. Oller, S. Malato, Appl. Catal. B: Environ. 125 (2012) 51–58.
[13] J. Feng, A. Xijun Hu, P.L. Yue, Environ. Sci. Technol. 38 (2004) 5773–5778.
[14] J. Ma, W. Song, C. Chen, W. Ma, J. Zhao, Y. Tang, Environ. Sci. Technol. 39 (2005) 5810–5815.
[15] P. Singh, P. Raizada, S. Kumari, A. Kumar, D. Pathania, P. Thakur, Appl. Catal. A: Gen. 476 (2014) 9–18.
[16] F.C. Moreira, A.R.B. Rui, E. Brillas, V.J.P. Vilar, Environ. Sci. Technol. 162 (2015) 34–44.

[17] S. Giannakis, M.I.P. López, D. Spuhler, J.A.S. Pérez, P.F. Ibáñez, C. Pulgarin, Appl. Catal. B: Environ. 199 (2016) 199–223.
[18] L. Chen, J. Ma, X. Li, J. Zhang, J. Fang, Y. Guan, P. Xie, Environ. Sci. Technol. 45 (2011) 3925–3930.
[19] C.K. Duesterberg, T.D. Waite, J. Catal. 41 (2007) 4103–4110.
[20] N. Wang, L. Zhu, M. Lei, Y. She, M. Cao, H. Tang, ACS Catal. 1 (2011) 1193–1202.
[21] T. Xu, R. Zhu, J. Zhu, X. Liang, Y. Liu, Y. Xu, H. He, Appl. Clay Sci. 129 (2016) 27–34.
[22] X. Yang, W. Chen, J. Huang, Y. Zhou, Y. Zhu, C. Li, Sci. Rep. 5 (2015).
[23] A. Fujishima, T.N. Rao, D.A. Tryk, J. Photochem. Photobiol. C: Photochem. Rev. 1 (2000) 1–21.
[24] X. Li, A. Chuncheng Chen, J. Zhao, Langmuir 17 (2001) 4118–4122.
[25] M. Ge, L. Liu, W. Chen, Z. Zhou, CrystEngComm 14 (2012) 1038–1044.
[26] L. Ge, K. Moor, B. Zhang, Y. He, J.H. Kim, Nanoscale 6 (2014) 13579–13585.
[27] D.E. Latta, B. Mishra, R.E. Cook, K.M. Kemner, M.I. Boyanov, Environ. Sci. Technol. 48 (2014) 1683–1691.
[28] A.E. Harvey, J.A. Smart, E.S. Amis, Anal. Chem. 27 (1955) 26–29.
[29] J. Yu, W. Wang, B. Cheng, B.L. Su, J. Phys. Chem. C 113 (2009) 6743–6750.
[30] R.O. Olojo, R.H. Xia, A. Jj, Anal. Biochem. 339 (2005) 338–344.
[31] S. Das, M.J. Hendry, J. Essilfiedughan, Environ. Sci. Technol. 45 (2011) 5557–5563.
[32] T. Xu, R. Zhu, J. Liu, Q. Zhou, J. Zhu, X. Liang, Y. Xi, H. He, J. Mol. Catal. A: Chem. 424 (2016) 393–401.
[33] S. Obregón, G. Colón, Appl. Catal. B: Environ. 158–159 (2014) 242–249.
[34] I. Grigioni, K.G. Stamplecoskie, E. Selli, P.V. Kamat, J. Phys. Chem. C 119 (2015) 20792–20800.
[35] Q. Kang, J. Cao, Y. Zhang, L. Liu, H. Xu, J. Ye, J. Mater. Chem A 1 (2013) 5766–5774.
[36] K. Sayama, K. Mukasa, R. Abe, Y. Abe, H. Arakawa, J. Photochem. Photobiol. A: Chem. 148 (2002) 71–77.
[37] J. Ma, W. Song, C. Chen, W. Ma, J. Zhao, Y. Tang, Environ. Sci. Technol. 39 (2005) 5810–5815.
[38] T. Tong, J. Zhang, B. Tian, F. Chen, D. He, J. Hazard. Mater. 155 (2008) 572–579.
[39] T. Xu, R. Zhu, J. Zhu, X. Liang, Y. Liu, Y. Xu, H. He, Catal. Sci. Technol. 6 (2016) 4116–4123.
[40] Y. Lee, W. Lee, J. Hazard. Mater. 178 (2010) 187–193.
[41] C.H. Lee, T.S. Lin, C.Y. Mou, Phys. Chem. Chem. Phys. 4 (2002) 3106–3111.
[42] Z. Hui, L. Zhao, F. Geng, L.H. Guo, B. Wan, Y. Yu, Appl. Catal. B: Environ. 180 (2016) 656–662.
[43] Y. Gao, Y. Wang, H. Zhang, Appl. Catal. B: Environ. 178 (2015) 29–36.
[44] T. Tachikawa, T. Ochi, Y. Kobori, ACS Catal. 6 (2016) 2250–2256.
[45] Y. Yang, Y. Guo, F. Liu, X. Yuan, Y. Guo, S. Zhang, W. Guo, M. Huo, Appl. Catal. B: Environ. 142–143 (2013) 828–837.
[46] A. Babuponnusami, K. Muthukumar, Chem. Eng. J. 183 (2012) 1–9.